Title

The BDNF mimetic R-13 attenuates TBI pathogenesis using TrkB-related pathways and bioenergetics

Journal

Biochimica et Biophysica Acta (BBA) - Molecular Basis of Disease, 1869(7)

ISSN

0925-4439

Authors

Thapak, Pavan
Smith, Gregory
Ying, Zhe
et al.

Publication Date

2023-10-01

DOI

10.1016/j.bbadis.2023.166781

Peer reviewed

Published in final edited form as:

Biochim Biophys Acta Mol Basis Dis. 2023 October ; 1869(7): 166781. doi:10.1016/j.bbadis.2023.166781.

The BDNF mimetic R-13 attenuates TBI pathogenesis using TrkB-related pathways and bioenergetics

Pavan Thapak[a], **Gregory Smith**[b,c], **Zhe Ying**[a], **Afshin Paydar**[b,c], **Neil Harris**[b,c,d], **Fernando Gomez-Pinilla**[a,b,c,*]

[a]Dept. Integrative Biology and Physiology, UCLA, Los Angeles, CA, United States of America

[b]Department of Neurosurgery, UCLA David Geffen School of Medicine, Los Angeles, CA, United States of America

[c]UCLA Brain Injury Research Center, Los Angeles, CA, United States of America

[d]Intellectual Development and Disabilities Research Center, University of California at Los Angeles, Los Angeles, CA 90095, USA

Abstract

Traumatic brain injury (TBI) is major neurological burden globally, and effective treatments are urgently needed. TBI is characterized by a reduction in energy metabolism and synaptic function that seems a primary cause of neuronal dysfunction. R13, a small drug and BDNF mimetic showed promising results in improving spatial memory and anxiety-like behavior after TBI. Additionally, R13 was found to counteract reductions in molecules associated with BDNF signaling (p-TrkB, p-PI3K, p-AKT), synaptic plasticity (GluR2, PSD95, Synapsin I) as well as bioenergetic components such as mitophagy (SOD, PGC-1α, PINK1, Parkin, BNIP3, and LC3) and real-time mitochondrial respiratory capacity. Behavioral and molecular changes were accompanied by adaptations in functional connectivity assessed using MRI. Results highlight the potential of R13 as a therapeutic agent for TBI and provide valuable insights into the molecular and functional changes associated with this condition.

Keywords

Fluid percussion injury; Mitophagy; Mitochondrial bioenergetics; Synaptic plasticity; Brain-derived neurotrophic factor (BDNF); Tropomyosin receptor kinase B (TrkB)

*Corresponding author at: Department of Integrative Biology & Physiology, University of California at Los Angeles (UCLA), 621 Charles E. Young Drive South, Los Angeles, CA 90095, USA. fgomezpi@ucla.edu (F. Gomez-Pinilla).

CRediT authorship contribution statement

Pavan Thapak: Conceptualization, Experimental work, Methodology, Formal analysis, Investigation, Writing– original draft of manuscript and preparation of final draft. **Gregory Smith:** Data acquisition, Formal analysis, Writing. **Lily Ying:** Technical supervision, Tissue collection. **Afshin Paydar:** Investigation. **Neil Harris:** Project administration, Supervision, Writing – review & editing. **Fernando Gomez-Pinilla:** Conceptualization, Project administration, Supervision, Writing – review & editing, Funding acquisition.

Declaration of competing interest

The authors declare that they have no competing financial and personal interest that would influence the work reported in this paper.

1. Introduction

Traumatic brain injury (TBI) leads to long-term neurological infirmities and remains an unsolved health calamity affecting domestic, military, and sporting environments worldwide [1,2]. The reduction in mitochondrial capacity and synaptic plasticity are key factors contributing to cell dysfunction after TBI. There is an urgent need to implement new pharmacological applications to foster functional connections after TBI. R13 (7,8-Bis(((methylamino)carbonyl)oxy)-2-phenyl-4H-1-benzopyran-4-one; M.W.: 368.34 g/mol) is a 7,8-dihydroxyfavone (7,8-DHF) prodrug and mimetic of brain-derived neurotrophic factor (BDNF) that is gaining attention as a potential pharmacological agent. R13 has a much better bioavailability and pharmacokinetic profile than 7,8-DHF [3]. Although BDNF has shown efficacy in several animal models of neurodegenerative disorders, its poor pharmacological profile has restricted its therapeutic implementation. In turn, the BDNF analog R13 has a small molecular size and prominent pharmacokinetic profile [3,4]. R13 releases 7,8-DHF into the circulatory system and binds to the TrkB receptor extracellular domain composed of cysteine cluster 2 and the leucine-rich region, and the Ig2 domain of the TrkB-D5 extracellular domain. BDNF binding to TrkB receptor is partly mediated through the Ig2 domain of the receptor which contributes to the receptor dimerization [5,6].

We wanted to assess the potential therapeutic efficacy of R13 by focusing on main events occurring during the TBI pathology. Mitochondrial dysfunction can lead to acute energy failure, infammation, and loss of synaptic plasticity, mitophagy, and others [7,8]. Mitophagy is gaining attention due to its ability to preserve mitochondrial homeostasis in several neurological disorders. Mitophagy is an autophagic response that selectively removes damaged mitochondria necessary to facilitate functional recovery [9–11]. Activation of TrkB, a BDNF receptor, plays a crucial role in autophagy regulation [12,13]. R13 as a BDNF analog may help to prevent dysfunctional mitophagy and improve outcomes after TBI.

Loss of cognitive function is also a major hallmark of TBI, which is accompanied by deficits in synaptic plasticity and mitochondrial bioenergetics [3,14,15]. R13 has shown efficacy to attenuate age-related attenuation of cortical synaptic plasticity in a similar fashion as BDNF [16]. In addition, R13 demonstrated potential to improve cognitive function in an animal model of Alzheimer's disease [3], suggests that R13 may also be beneficial for TBI. R13, as a mimetic of BDNF, may have a dual potential to influence both synaptic plasticity and metabolism. Therefore, in this study, we evaluate the effects of R13 to improve hippocampal-based function, including synaptic plasticity and mitochondrial bioenergetics and mitophagy components following TBI. Resting-state functional magnetic resonance imaging is used to assess functional outcomes and the underlying mechanisms that may contribute to altered brain plasticity and its improvement after TBI.

2. Material and methods

2.1. Animals and treatments

Male adult Sprague–Dawley rats (200 g–220 g) were purchased from Charles River Laboratories, Wilmington, MA and housed in standard polyacrylic cages. All animals

were housed individually in 12 h light and dark cycle with food and water ad libitum under standard housing temperature (22 ± 2 °C). All experiments were performed in compliance with the United States National Institutes of Health Guide for the Care and Use of Laboratory Animal after the approval of the UCLA Chancellor's Animal Research Committee.

Rats were acclimatized in the vivarium for 7 days after delivery. They received two learning trial on the Barnes maze per day for 5 days. Immediately after the final trial on day 5, a fluid percussion or sham injury was conducted, and impact pressure and apnea time were recorded. MRI data were acquired at 24 h after injury, after which injured rats received either R13 (7.25 mg/kg, i.p, $n = 5$) or vehicle (5 % DMSO in PBS: saline (1:1), $n = 7$) for 7 consecutive days [3]. A probe trial was conducted on the Barnes maze on day 6 post-injury. Elevated plus maze was run on the following day (7 days post-injury), immediately after which MRI data was acquired. Another set of animals ($n = 6$) were used for the analysis of mitochondrial bioenergetics at 3rd-day post-injury. All animals were euthanized, and the ipsilateral hippocampus was isolated for further biochemical analysis. Animals were randomly assigned to the following groups: Sham animals treated with vehicle (Sh + V), TBI animals treated with vehicle (TBI + V), and TBI animals treated with R13 (TBI + R13). Each group consisted of 5 to 7 animals (Fig. 1).

2.2. Fluid percussion injury (FPI)

A fluid percussion injury or sham injury was conducted as described previously [15]. In brief, animals were anesthetized with isoflurane (4 %, vaporized in oxygen) which was maintained at 2 % for general levels of anesthesia while the rat was in a stereotaxic frame and temperature maintained via homeothermic control using a thermal pad. Eye ointment was applied, and a midline sagittal incision was made on the head to expose the skull, following which a 5 mm craniectomy was made over the left parietal cortex (AP = 4.5 mM Midline to left = 2.5 mm) using a hand trephine. A plastic injury hub (5 mm) was fixed on the outside of craniectomy around the exposed dura mater and sealed with dental cement. Sterile saline was used to fill the injury hub which was directly connected to the fluid reservoir of the FPI device. Anesthesia was temporarily discontinued, and rats received a moderate impact using an arm angle of 24° which corresponded to a peak pressure wave of 2.5 ± 0.2 atm. Apnea duration and time for righting refex to return were recorded. Anesthesia was reinstated in order to suture the skin and to apply topical antibiotic to the wound site. The same surgical procedures were conducted on sham rats except for FPI.

2.3. Barnes maze (BM)

Assessment of memory was performed using the Barnes maze task. The apparatus consists of a circular table (115 cm in diameter), 7 cm circular holes evenly spaced at the edge of the apparatus. During all learning trials, an escape box was placed underneath the same hole. Two trials were run per day with a 15 min interval and for five consecutive days before sham or FPI injury was conducted. The learning trials were completed by either the animal finding the escape box or 300 s had elapsed. Trials were conducted in the presence of bright light as an aversive stimulus which created a uniform illumination on the table of 6000 lm. If rats were not able to find the escape box on the first day, they were manually moved to

the escape box for 15 s. On the 6th day of injury, animals received a probe trial and time to find escape box was recorded by ANY-maze software (Stoelting Co., USA). The surface of the apparatus was cleaned thoroughly between trials with 70 % alcohol to remove olfactory signs and 3 special cues (shape) were used during the study [14].

2.4. Elevated plus-maze (EPM)

The elevated plus maze behavioral assay is used for the assessment of anxiety-like behavior. It is plus shape apparatus elevated (60 cm) from the ground and consists of two closed arms and two open arms (10 × 50 cm). On the 7th day of surgery, each animal was individually kept in the center of the EPM facing the open arm, and distance and time spent in the open arm was recorded for 5 min by ANY-maze software (Stoelting Co., USA). After completion of the task animals were returned to the home cage and the apparatus was cleaned thoroughly with 70 % alcohol properly before beginning the next trial [17,18].

2.5. Immunoblotting

The hippocampus ipsilateral to the injury was isolated on the 7th day post-TBI and homogenized in lysis buffer (50 mM Tris-HCl, 157 mM NaCl, 10 % glycerol, 1 % NP-40, 1 μl/ml protease inhibitor cocktail). Protein estimation was carried out by Barford assay. NuPAGE Bis-Tris Midi gel (10–12 %) (Thermo Fisher Scientific, MA, USA) was used to separate an equal amount of protein and transblotted to PVDF membrane (Bio-Rad, Hercules, CA, USA). The membrane was incubated for 60 min at room temperature in 5 % BSA to block the non-specific proteins. After blocking, the membrane was incubated with primary antibodies BDNF (Santacruz Biotechnology, CA, USA, Cat#sc-546, 1:500), p-TrkB (Tyr-816) (Merk Millipore, MA, USA; Cat#ABN1381; 1:500), TrkB (Cell signaling Technology, MA, USA, Cat#4603S, 1:1000), p-PI3K (Cell signaling Technology, MA, USA, Cat#17366S), PI3K (Cell signaling Technology, MA, USA, Cat# 4249S), p-Akt (Ser-473) (Cell signaling Technology, MA, USA, Cat# 4058S, 1:1000), Akt (Cell signaling Technology, MA, USA, Cat#9272S, 1:1000), tPA (Proteintech, IL, USA, Cat#10147–1-AP, 1:2000), GluR2 (Santacruz Biotechnology, CA, USA, Cat# sc-517,265, 1:1000), PSD95 (Cell Signaling Cat#3450×, 1:1000), Synapsin I (Santa Cruz Biotechnology, CA, USA, Cat#sc-376,623, 1:2000), p-CREB (Thermo Fisher Scientific, MA, USA, Cat#PA1–4619, 1:2000), CREB (MiliporeSigma, MA, USA, Cat#06–863, 1:2000), PGC-1α (Invitrogen, MA, USA, Cat#PA5–72948, 1:2000), SOD (Cell signaling Technology, MA, USA, Cat#13141S, 1:2000), PINK1 (Santacruz Biotechnology, CA, USA, Cat#sc-517,353, 1:1000), Parkin (Santacruz Biotechnology, CA, USA, Cat#sc-32,282, 1:1000), BNIP3 (Cell signaling Technology, MA, USA, Cat#3769S, 1:2000), MAP-LC3β (Santacruz Biotechnology, CA, USA, Cat# sc-271,625, 1:1000), β-actin (Santacruz Biotechnology, CA, USA, Cat#sc-47,778, 1:1000) at 4 °C overnight. After washing with tris-buffered saline-tween-20 (0.1 %) (TBST), the membrane was incubated with horseradish peroxidase (HRP)-conjugated secondary antibody (1:10,000) for 90 min at RT. The membrane was rinsed by TBST and incubated in enhanced chemiluminescence to visualize the bound antibody. Densitometry was performed by ImageJ software to quantify the relative band intensity [19].

2.6. Mitochondrial activity assay

Mitochondria was isolated from ipsilateral hippocampus and homogenized in ice-cold MSHE buffer (70 mM sucrose, 220 mM mannitol, 5 mM KH2PO4, 5 mM MgCl2, 1 mM EGTA, 0.2 % BSA, 2 mM HEPES pH 7.3) on 3rd-day post-TBI. All homogenates were centrifuged at 2000*g* for 3 min at 4 °C. The supernatant was collected and centrifuged at 12000*g* at 4 °C for 10 min, and pellets were resuspended in MSHE buffer containing 0.2 % digitonin and centrifuged at 12000*g* at 4 °C for 10 min. The mitochondria were washed with MSHE buffer without BSA and again centrifuged at 12000*g* at 4 °C for 10 min and final mitochondrial palettes were resuspended in 25–30 uL MSHE buffer (without BSA and digitonin). Protein concentration was estimated by BCA method.

A Seahorse XF96 (Seahorse Bioscience, MA, USA) was used to measure of mitochondrial oxygen consumption. Isolated mitochondria were plated at 3μg/well for Complex I substrates and 2.5μg/well for Complex II substrates and centrifuged onto the plate at 2100 x*g* for 5 min at 4 °C. Complex I-driven respiration was measured with pyruvate (5 mM) + malate (5 mM) as substrates, while Complex II with succinate (5 mM) and 2uM rotenone to inhibit Complex I. Injections during the assay included final concentration of 4 mM ADP (State 3 respiration), 3 uM oligomycin (State 4o), 3 uM FCCP (uncoupled), and 4 uM antimycin A to inhibitor mitochondrial respiration. The oxygen consumption rate (OCR) data was normalized to ug protein per well before analysis of complex-1 and II-dependent respiration was assessed [20].

2.7. Magnetic resonance imaging (MRI)

2.7.1. MRI acquisition—All MRI data were acquired on a 7 T magnet interfaced to Bruker console running Paravision 5.1 and BGA-12 gradients with a maximum strength of 400mT/m (Bruker, Billerica, MA). A quadrature, receive-only surface coil (Rapid MRI International, Columbus, Ohio) actively decoupled from a whole-body birdcage coil (Bruker, Billerica, MA) used in transmit mode was used to acquire the data. For each scan session animals were briefly anesthetized with 5 % isoflurane vaporized in oxygen delivered at 0.8 l/min before receiving an intraperitoneal bolus injection of dexmedetomidine (0.05 mg/kg). The isoflurane was adjusted to 0.5 % and a continuous, subcutaneous influsion of dexmedetomidine (0.1 mg/kg/h) was begun. Animals were monitored and homeothermically maintained at 37 °C via external, forced air heating. Respiration rate was monitored and maintained in a range of 40–60 breath per minute through minor adjustments of isoflurane concentration.

A standard multi-echo gradient echo 3D sequence was used to acquire T2/T2*-weighted structural images using: a repetition time (TR) of 125 ms, and 13 echoes with an effective echo time (TE) range of 2.8–52 ms and 4.08 ms echo spacing, a 20° fip angle and a data matrix and field of view that resulted in a 160 mm^3 isometric voxel resolution. Gradient echo, echo planar resting state functional MRI (rsfMRI), data were continuously acquired for 15 min beginning at 30 min after dexmedetomidine/0.5 % isoflurane was begun using the following parameters:450 repetitions at a TR/TE of 2000/16 ms and a data matrix of 96 × 96 and 25 coronal slices, resulting in an in-plane resolution of 0.3125 × 0.3125mm^3 and 0.75 mm slice thickness. 10 dummy scans were obtained at the beginning of each acquisition.

2.7.2. MRI analysis—Functional MRI data were processed as before by us in an automated pipeline [14,21–23] using motion correction, gaussian spatial smoothing to 0.5 of full width half maximum, band passed-filtered between 0.01 and 0.25 Hz and Gaussian smoothed to 0.2 mm [24–26]. All data were co-registered to an unbiased template constructed from all the data using ANTS. Function seed analysis of the left hippocampus was preformed using FSL Feat, the seed was selected based on a co-registered atlas [23,27,28]. The change in connectivity from 1d to 7d post-injury using a fixed-effects analysis of the difference from T2 minus T1 on a voxel-by-voxel comparison using FEAT. Next, a mixed effect analysis for group comparison of voxel-by-voxel analysis using apnea (seconds) at the time of injury as nuisance covariate was conducted in FEAT. Difference over time and between groups were determined based on uncorrected data with a minimum z value of 1.7 (P 0.05).

Anatomical analysis of atrophy and expansion images were first normalized and corrected using N4 bias correction following brain extraction and co-registering each animal to an unbiased mean space brain template constructed using Advanced Normalization Tools [29]. Utilizing the Jacobian determinant from the co-registration mean and standard deviation maps for the sham group were created on a voxel-by-voxel basis. For each animal a z-map was calculated by comparing to the sham group for each voxel. Based on a co-registered atlas the left hippocampus was selected as the ROI. Volumes of tissue compression/atrophy were measured using the volume of the negative local tissue deformation within in ROI, and tissue expansion/swelling is based on the positive local tissue deformation.

2.8. Statistical analysis—Data are expressed as Mean ± S.E.M. Statistical significance among the diverse groups was analyzed by one-way analysis of variance (ANOVA) followed by post hoc analysis using Tuckey's test (GraphPad Prism 7, Boston, MA). Behavioral data was analyzed by ANOVA followed by non-parametric post hoc analysis using Dunn's test. A significant difference was considered at P 0.05. Correlation analysis was performed by Pearson correlation to evaluate association between variables.

3. Results

3.1. R13 intervention counteracts the memory dysfunction and anxiety-like behavior after TBI

At post-injury day 6 there was an increase in the latency to find the escape box in injured-vehicle treated rats compared to sham (p 0.05) while daily R13 administration from day 1 post-injury significantly reduced the effect of injury on the latency time compared to vehicle treatment (p 0.05) (Fig. 2B). To assess the anxiety effect post-TBI, animals were evaluated on the EPM. In TBI-vehicle rats there was a reduction in the time spent (p 0.05) and distance travelled (p 0.05) in the open arm as compared to sham-operated, while R13 administration significantly normalized both the time spent (p 0.05) (Fig. 2C) and distance travelled ($p >$ 0.05) in the open arm compared to vehicle treated, injured rats (Fig. 2D).

3.2. R13 intervention enhances BDNF/TrkB signaling cascade following TBI

TBI-vehicle reduced mature form of brain derived neurotropic factor (mBDNF) ($F_{(2, 14)}$ = 14.99, p = 0.003) while pro-BDNF level ($F_{(2, 14)}$ = 4.99, p = 0.037) was increased as compared to sham-operated animals. However, R13 intervention counteracted TBI effects and enhanced mBDNF ($F_{(2, 14)}$ = 14.99, p = 0.003) level while decrease pro-BDNF level ($F_{(2, 14)}$ = 4.99, p = 0.03). Interestingly, we found a negative correlation between mBDNF (r = 0.635, p 0.01) levels vs BM latency (Fig. 3B–D). Tissue plasminogen activator (tPA) is involved in the formation of mature BDNF (mBDNF) from pro-BDNF sources. TBI reduced tPA levels ($F_{(2, 14)}$ = 6.36, p = 0.009), while R13 treatment restored tPA ($F_{(2, 14)}$ = 6.36, p = 0.03) levels (Fig. 3E).

We assessed the phosphorylation of TrkB receptor and associated downstream molecules. TBI reduced levels of p-TrkB (Tyr 816) receptor phosphorylation ($F_{(2, 14)}$ = 15.0, p = 0.02) as compared to sham animals while treatment with R13 counteracted the action of TBI and increased p-TrkB (Tyr 816) level ($F_{(2, 14)}$ = 15.0, p = 0.0002) (Fig. 3F). We assessed the interaction between mBDNF and p-TrkB and found a positive correlation (r = 0.77, P 0.001) (Fig. 3G). We also assessed protein levels of PI3K and Akt which are associated with TrkB signaling. TBI reduced levels of phosphorylated PI3K ($F_{(2, 14)}$ = 8.45, p = 0.02) and Akt ($F_{(2, 14)}$ = 7.63, p = 0.03) while R13 treatment counteracted the TBI effect by increasing the phosphorylation of P13K ($F_{(2, 14)}$ = 8.45, p = 0.003) and Akt ($F_{(2, 14)}$ = 11.56, p = 0.001) (Fig. 3H, I).

3.3. R13 intervention normalizes the alteration in synaptic plasticity markers following TBI

Cognitive performance declined with impairments of synaptic plasticity. PSD-95 and GluR2 contribute to synaptic plasticity by maintaining the activity of ionotropic receptors at the synapse. TBI animals showed a reduction in PSD-95 ($F_{(2, 14)}$ = 10.48, p = 0.041), and GluR2 ($F_{(2, 14)}$ = 6.90, p = 0.02) levels, however, R13 intervention increased PSD-95 ($F_{(2, 14)}$ = 10.48, p = 0.001), and GluR2 ($F_{(2, 14)}$ = 6.90, p = 0.04), levels in TBI animals. In addition, we also measured protein levels of phosphorylated CREB (ser-133), which is a transcription factor crucially involved in memory formation. TBI animals showed a reduction in the protein level of p-CREB ($F_{(2, 14)}$ = 7.76, p = 0.03) while treatment with R13 enhanced p-CREB ($F_{(2, 14)}$ = 7.76, p = 0.004) in TBI animals (Fig. 3J–L). Synapsin I, a vesicle-associated essential presynaptic protein has a key role in cognition enhancement which was reduced ($F_{(2, 14)}$ = 9.82, p = 0.008) after TBI and counteracted ($F_{(2, 14)}$ = 9.82, p = 0.0027) by R13 intervention (Fig. 3M).

3.4. R13 intervention improves mitochondrial bioenergetics following TBI

Brain energy deprivation is a hallmark of TBI which involves mitochondrial dysfunction. Therefore, we measured oxygen consumption rate (OCR) in isolated ipsilateral hippocampal mitochondria at 72 h after moderate FPI injury. We measured OCR in real-time in the presence of sequential treatment of respiratory modulators. Our findings revealed a reduction in the Complex I associated respiration state 3 ($F_{(2, 15)}$ = 6.54, p = 0.015) (Fig. 4B), state 4 respiration ($F_{(2, 15)}$ = 3.46, p = 0.25) (Fig. 4C) and uncoupled respiration ($F_{(2, 15)}$ = 7.82, p = 0.024) (Fig. 4D) in TBI animals. State 3 respiration provides an indication

of utilization of ADP to generate ATP while state 4 respiration state represents the proton gradient status during mitochondrial respiration. Uncoupled or state V respiration represents maximum respiratory capacity of mitochondrial functioning. R13 intervention neutralized these TBI effects for consecutive 3 days and enhanced the Complex I mediated respiration states (state 3 ($F_{(2, 15)}$ = 6.54, p = 0.012), uncoupled ($F_{(2, 15)}$ = 7.82, p = 0.003) and state 4 ($F_{(2, 15)}$ = 3.46, p = 0.038)) after TBI. We also measured respiration via Complex II using succinate and rotenone substrate and we observed that TBI decreased state 3 ($F_{(2, 15)}$ = 4.80, p = 0.036) (Fig. 4F), state 4 ($F_{(2, 15)}$ = 2.94, p = 0.092) (Fig. 4G) and uncoupled ($F_{(2, 15)}$ = 4.6, p = 0.038) (Fig. 4H). R13 intervention restored complex II-mediated respiration (state 3 ($F_{(2, 15)}$ = 4.80, p = 0.031), state 4 ($F_{(2, 15)}$ = 2.94, p = 0.11) and uncoupled ($F_{(2, 15)}$ = 4.6, p = 0.037) in TBI animals.

3.5. R13 intervention preserves mitochondrial homeostasis and ameliorates reductions in mitophagy markers post-TBI

PGC-1α is a transcriptional factor involved in mitochondrial biogenesis. TBI-Vehicle reduced levels of PGC-1α ($F_{(2,13)}$ = 9.069, P = 0.05) as compared to sham animals while R13 treatment normalized PGC-1α levels ($F_{(2, 13)}$ = 9.069, p = 0.002) in TBI afflicted animals (Fig. 5B). We assessed the interaction between PGC-1α and latency and found that the mitochondrial biogenesis marker PGC-1α is inversely related to the BM latency (r = 0.705, P 0.01) (Fig. 5D). TBI also reduced levels of SOD ($F_{(2, 14)}$ = 5.22, P = 0.03) as compared to sham animals. However, R13 treatment counteracted the TBI effects and enhanced the SOD level ($F_{(2, 14)}$ = 5.22, P = 0.02) in TBI animals (Fig. 5C). SOD is an antioxidant enzyme that neutralizes the reactive oxygen species generated in mitochondria during ATP synthesis.

TOM20 is a mitochondrial outer membrane protein involved in mitochondrial homeostasis. TBI increased TOM20 mitochondrial homeostasis. TBI increased TOM20 ($F_{(2, 14)}$ = 5.26, p = 0.04) level while R13 treatment counteracted the TBI effect on TOM20 ($F_{(2, 14)}$ = 5.26, p = 0.02) level. TBI animals showed a reduction in mitophagy markers PINK1 ($F_{(2, 14)}$ = 19.29, p = 0.007), Parkin ($F_{(2, 14)}$ = 8.73, p = 0.003). MAP-LC3β ($F_{(2, 14)}$ = 7.5, p = 0.02) and BNIP3 ($F_{(2, 14}$ = 15.12, p = 0.0004). R13 intervention enhanced mitophagy markers PINK1 ($F_{(2, 14)}$ = 19.29, p = 0.0003), Parkin ($F_{(2, 14)}$ = 8.73, p = 0.01), MAP-LC3β ($F_{(2, 14)}$ = 7.50, p = 0.006) and BNIP3 ($F_{(2, 14)}$ = 15.12, p = 0.0004) in TBI animals (Fig. 5E–I). We correlated the mitophagy marker BNIP3 with latency and found a negative (r = 0.794, P 0.001) association (Fig. 5J). Conversely, we observed positive correlation between mBDNF and BNIP3 (r = 0.724, P 0.001) as well as SOD and BNIP3 (r = 0.670, p 0.01) (Fig. 5K, L).

3.6. MRI studies

The ipsilateral hippocampus was selected for exploratory seed analysis in order to provide a direct in vivo readout of the molecular data from the same region. The difference in connectivity from 1 to 7 days after injury was calculated for each rat to determine the mean increase in connectivity over the 6 days. Injury+ vehicle resulted in an increase in connectivity over the first week between the left hippocampus and the ipsilateral striatum and thalamus, as well as an increase to the contralateral S1 cortex compared to sham rats as well as numerous other regions (Fig. 6A). R13 treated injured rats displayed similar

increases in connectivity compared to shams (Fig. 6B), but notably a reduction in ventral caudate, S1 and piriform cortex, and additional bilateral increases in a granular insular cortex (Fig. 6C). These changes are summarized (Fig. 6D).

There was significant local tissue deformation within the left hippocampus after injury following either vehicle or R13 intervention when compared to the sham group (Fig. 7E). There was no significant effect of R13 on expansion or atrophy. However, R13-treated rats trended toward less atrophy and expansion by day 7.

4. Discussion

It is well-established that TBI can cause long-term neurological impairments and there is a pressing need to develop effective therapeutic strategies to reduce its pathogenesis. While BDNF has shown positive effects on neuronal survival and synaptic plasticity, its limited pharmacokinetics have hindered its therapeutic potential in TBI and other neurological disorders [30–32]. Dysregulation in the BDNF-TrkB axis is a common sequela after TBI. R13, a DHF prodrug that mimics the effects of BDNF, has emerged as a promising therapeutic alternative. The promise of R13 to reduce several aspects of TBI pathology roots from previous studies showing the efficacy of DHF in TBI pathogenesis [33–35]. Our results show that R13 intervention counteracted dysfunctions in cognition and anxiety-like behavior in conjunction with normalization of levels of BDNF and its TrkB receptor, improvements of mitochondrial activity and ATP formation. In addition, R13 counteracted reductions in critical elements of the autophagy pathway cascade that are associated with cell bioenergetics. These findings suggest that R13 has the potential to counteract key aspects of TBI pathogenesis and improve functional outcomes.

Given the role of BDNF in learning and memory, and reports that BDNF levels decline after TBI [36] we assessed molecular system related to the action of BDNF on synaptic plasticity and behavior. R13 treatment has a protective effect on various molecular systems related to BDNF action and synaptic plasticity, which in turn leads to improvements in behavioral performance in the Barnes maze and elevated plus-maze tasks. Specifically, R13 counteracted the TBI-induced decrease in GluR2, PSD95, Synapsin I, and p-CREB levels. BDNF potentiates synaptic function by regulating the expression of α-amino-3-hydroxy-5-methyl-4-isoxazoleproprionic acid (AMPA) receptors. GluR2 is a subunit of AMPA receptor which regulates the biophysical activity and trafficking of the AMPA receptor at the synapse, and our results show that TBI reduces GluR2 levels. PSD-95 is a synaptic scaffolding protein which supports synaptic function by increasing AMPAR-mediated synaptic transmission which enhances long-term potentiation [37–42]. In addition, the action of CREB has been involved in spatial memory and neuronal plasticity by influencing BDNF transcription [43,44]. We observed a decrease in levels of GluR2, PSD95, Synapsin I, and p-CREB (ser-133) in TBI, however, R13 intervention counteracted these effects. The binding of BDNF to TrkB receptor leads to activation of downstream signaling pathways including phosphatidylinositol 3-kinase (PI3K/Akt). Similarly, R13 initiates dimerization and autophosphorylation of TrkB receptor, with activation of PI3K/Akt signaling cascade [45,46]. In this study, R13 administration enhanced the phosphorylation of TrkB (Tyr-816), PI3K (Tyr-458), and Akt (ser-473) following TBI. TrkB-mediated PI3K-Akt is required for

the induction of synaptic remodeling and LTP [47,48] which are main elements for synaptic plasticity. These results suggest that R13 has the potential to improve cognitive function and synaptic plasticity after TBI, likely through its modulation of the BDNF-TrkB axis.

Besides the TrkB receptor, BDNF acts at lesser extent on p75 receptor (p75-NTR) in brain. BDNF is synthesized as pro-BDNF which undergoes proteolytic processing to form mBDNF. mBDNF specifically binds to TrkB while pro-BDNF binds to p75-NTR. In our study, TBI reduced mBDNF level while increased pro-BDNF level, and both effects were counteracted by R13 intervention. We also observed mBDNF level changed inversely proportional to the latency in BM while activation of p-TrkB was directly associated with mBDNF. Activation of TrkB receptor is consistent with the protective action of BDNF on neurons, neurogenesis, and long-term potentiation (LTP). In turn, the decreases in pro-BDNF is consistent with the action of p75-NTR receptor on cell death [47,49–51]. In addition, R13 counteracted the decrease of tissue plasminogen activator (tPA) levels in TBI animals. tPA plays a role on the conversion of pro- to mature BDNF [52,53]. Reports that tPA enhances LTP [53–55] suggests that R13-related tPA could contribute to the action of R13 on memory as observed in our study. In addition, as discussed below, the action of tPA on dissolving blood clots could play a role on TBI recovery.

TBI can harm neuronal plasticity by disrupting mitochondrial function [15,56,57]. Mitochondria bioenergetics is crucial for regulation of cell function such that in this study, TBI reduced Complex I and Complex II-mediated respiration important for ATP formation and this was restored by R13 intervention. Alteration in mitochondrial bioenergetics also increases reactive oxygen species and this process is mitigated by antioxidants like superoxide dismutase (SOD) during the ATP formation [58,59]. Our findings showed that PGC-1α and SOD protein levels were reduced in TBI animals, and these values were normalized by R13 treatment. BDNF plays a role in regulating mitochondrial homeostasis in diseases like Parkinson’s and diabetes and TBI [15,60–63]. The current findings indicate the distinct potential of R13 to counteract mitochondrial bioenergetics and mitochondrial ROS emission after TBI.

Mitophagy is crucial to preserve mitochondrial health by removing dysfunctional mitochondrial subproducts after brain injury. BNIP3, PINK1, and Parkin are associated with mitochondrial degradation by autophagy. BNIP3 induces mitochondrial translocation of dynamin-related protein 1 (Drp1), a protein involved in mitochondrial fission, and Drp1-mediated mitochondrial fission correlated with increased mitophagy [64–67]. Previous studies also showed that PINK1/Parkin are related to mitophagy [68]. The results of this study suggest that R13 supports mitophagy flux in the TBI pathogenesis by counteracting the reduction of mitophagy markers PINK1, Parkin, BNIP3, and MAP-LC3β post-TBI. PINK1 recruitment of Parkin is the first step in the initiation of mitophagy by ubiquitination of mitochondria. BNIP3 interacts with LC3β to regulate autophagosome formation and degradation of mitochondria [69]. The levels of BNIP3 were found to be directly proportional to mBDNF and SOD levels, while inversely related to BM latency indicating a link between mitophagy, antioxidant defenses, and cognitive function.

TOM20, a mitochondria homeostatic protein, has a strong interaction with mitophagy markers such as PINK1, which regulates mitochondria depolarization in the outer mitochondria membrane. The study observed that TBI increased levels of TOM20 while R13 treatment counteracted these effects. This suggests that TBI likely reduces elimination of damaged mitochondria that may enhance TOM20 level. R13 may also support mitophagy by acting on the PI3K/Akt pathways, which may influence mTORC1 activity through tuberous sclerosis complex 2 (TSC2). The inhibition of mTOR by rapamycin induces PINK1-mediated mitophagy, suggesting an association between mTORC1 and mitophagy [70,71]. In summary, R13 intervention may support mitochondrial homeostasis by enhancing mitophagy flux through the regulation of mitophagy markers, such as PINK1, Parkin, BNIP3, and MAP-LC3β, as well as modulating the PI3K/Akt pathway and mTORC1 activity. These findings suggest a potential therapeutic application of R13 in the treatment of TBI by supporting mitochondrial dynamics and bioenergetics.

Our in vivo imaging showed an association between R13 functional connectivity, and structural deformation following TBI. The injured hippocampus in R13-treated rats trended to show less tissue atrophy/compression as well as reduced local tissue swelling, or expansion as compared to vehicle-treated. Additionally, given that R13 is improving synaptic plasticity, as viewed through hippocampal protein assays, the functional connectivity (FC) of this improved synaptic activity was determined via seeding the left hippocampus and determining what connections between the hippocampus and the rest of the brain were functionally improved over time. Analysis of the rs-fMRI showed that R13 intervention increased functional connectivity from the ipsilateral hippocampus to the ipsilateral nucleus accumbens, striatum, and thalamus, and to the contralateral M1/S1, agranular insular, and retrosplenial cortices when compared to sham rats. The hippocampal and medial entorhinal cortex circuit is an important circuit in memory and spatial navigation. Additionally, the hippocampal piriform cortex has been shown to be involved in odor information incorporation [72,73]. The strengthened FC in these hippocampal circuits show that the R13 trended toward restored functional connection, and this was coincident with improved cognitive function after TBI. In other words, R13 treatment following injury results in improved synaptic and metabolic function in the hippocampus and this improvement in synaptic function improves the FC of the hippocampus in neurocircuits that are involved in the cognitive improvement observed in the R13 treatment group. The circuit comparison of R13 to vehicle-treated, injured rats indicate an increase in insular cortices, a region involved in executive functions such as emotion, decision making and social cognition. Increased connectivity is in general agreement with the plus maze test showing reduced anxiety. The mechanism for improved hippocampal connectivity and cognitive outcome by R13 is unclear but is likely to occur through multiple pathways. Given that functional connectivity has been shown to be a close correlate of neuronal activity [74–76], one likely candidate is enhancement of synaptic activity directly through the subcellular neurotrophic actions subsequent to TrkB receptor binding by R13 [3]. Alternatively, improved synaptic activity may also occur indirectly through local metabolic enhancement [77,78] given the major improvement in mitochondrial function shown herein. A post-injury relationship between reduced endogenous tPA levels and both altered cerebral blood flow and reduced white matter recovery have been reported [79–81]. Given the ability

of tPA to dissolve blood clots as used for the treatment of acute stroke [82], tPA may also be a factor in altering local changes in blood flow. Since the blood oxygenation-level dependent (BOLD) signal is also associated with blood flow changes [83], a reduction in tPA could influence the regional correlation of BOLD signal and changes in functional connectivity. The role of tPA in altering local changes in blood flow and its potential influence on BOLD signal and changes in functional connectivity following TBI warrants further investigation.

R13 is a prodrug of 7,8-DHF which is a potent and selective agonist of TrkB receptor. Thereby playing a crucial role in neuronal plasticity and fostering mitochondrial activity resulting in neuronal protection from the insult. Moreover, earlier findings also manifest protective effects of neurological disorders such as ALS, AD [3,84]. Recombinant BDNF has shown limited ability as an intervention to improve functional outcomes due to its short half-life, as experienced in phase III clinical trial for ALS [85]. In turn, R13 has excellent oral bioavailability as well as a half-life profile in comparison to BDNF. Thus, R13 has strong clinical prospective and translational potential from bench to bed.

In summary, R13 was found to have multiple beneficial effects on the brain after TBI, including improving cognitive functions, reducing anxiety-like behavior, enhancing mitochondrial function and mitophagy, involving the TrkB/PI3K/Akt signaling pathway (Fig. 8). In addition, R13 intervention attenuates atrophy and enhances functional connectivity via restoring neuronal connections and neurovascular coupling. These results suggest that R13 may be a promising therapeutic option for the treatment of TBI.

Acknowledgments

This work was supported by the National Institutes of Health (grant numbers: NS111378, NS117148, NS116383). We are also thankful to Prof. Keqiang Ye for providing the R13 as a gift sample.

Data availability

Data will be provided on request.

Abbreviations:

TBI	traumatic brain injury
FPI	fluid percussion injury
BDNF	brain-derived neurotrophic factor
TrkB	tyrosine kinase B
PI3K	phosphoinositide 3-kinase
AKT	protein kinase B
GluR2	glutamate ionotropic receptor AMPA type subunit 2
PSD95	postsynaptic density protein 95
SOD	superoxide dismutase

PGC-1α	peroxisome proliferator-activated receptor-gamma coactivator-1alpha
PINK1	PTEN Induced Kinase 1
Parkin	E3 ubiquitin-protein ligase
BNIP3	BCL2/adenovirus E1B 19 kDa protein-interacting protein 3
MAP-LC3β	microtubule-associated proteins-light chain 3 beta
DMSO	Dimethyl sulfoxide
PBS	phosphate buffered saline
fMRI	functional Magnetic resonance imaging
7,8-DHF	7,8-dihydroxyfavone
AMPAR	α-amino-3-hydroxy-5-methyl-4-isoxazolepropionic acid
LTP	long-term potentiation
p75-NTR	p75 neurotrophin receptor
CREB	cAMP-response element binding protein
tPA	tissue plasminogen activator
ATP	adenosine triphosphate via TOM20 translocase of outer mitochondrial membrane 20
mTOR	mammalian target of rapamycin
BOLD	blood oxygenation-level dependent

References

[1]. Fischer TD, Hylin MJ, Zhao J, Moore AN, Waxham MN, Dash PK, Altered mitochondrial dynamics and TBI pathophysiology, Front. Syst. Neurosci 10 (2016), 10.3389/fnsys.2016.00029.

[2]. Kim S, Han SC, Gallan AJ, Hayes JP, Neurometabolic indicators of mitochondrial dysfunction in repetitive mild traumatic brain injury, Concussion. 2 (2017) CNC45, 10.2217/cnc-2017-0013.

[3]. Chen C, Wang Z, Zhang Z, Liu X, Kang SS, Zhang Y, Ye K, The prodrug of 7,8-Dihydroxyflavone development and therapeutic efficacy for treating Alzheimer's disease, Proc. Natl. Acad. Sci 115 (2018) 578–583, 10.1073/pnas.1718683115. [PubMed: 29295929]

[4]. Liu X, Qi Q, Xiao G, Li J, Luo HR, Ye K, O-methylated metabolite of 7,8-Dihydroxyflavone activates TrkB receptor and displays antidepressant activity, Pharmacology. 91 (2013) 185–200, 10.1159/000346920. [PubMed: 23445871]

[5]. Jang S-W, Liu X, Yepes M, Shepherd KR, Miller GW, Liu Y, Wilson WD, Xiao G, Blanchi B, Sun YE, Ye K, A selective TrkB agonist with potent neurotrophic activities by 7,8-dihydroxyflavone, Proc. Natl. Acad. Sci 107 (2010) 2687–2692, 10.1073/pnas.0913572107. [PubMed: 20133810]

[6]. Chitranshi N, Gupta V, Kumar S, Graham S, Exploring the molecular interactions of 7,8-Dihydroxyflavone and its derivatives with TrkB and VEGFR2 proteins, Int. J. Mol. Sci 16 (2015) 21087–21108, 10.3390/ijms160921087. [PubMed: 26404256]

[7]. Ng SY, Lee AYW, Traumatic brain injuries: pathophysiology and potential therapeutic targets, Front. Cell. Neurosci 13 (2019), 10.3389/fncel.2019.00528.

[8]. Zhang L, Wang H, Autophagy in traumatic brain injury: a new target for therapeutic intervention, Front. Mol. Neurosci 11 (2018), 10.3389/fnmol.2018.00190.

[9]. Chen G, Kroemer G, Kepp O, Mitophagy: an emerging role in aging and age-associated diseases, Front Cell Dev Biol. 8 (2020), 10.3389/fcell.2020.00200.

[10]. Chao H, Lin C, Zuo Q, Liu Y, Xiao M, Xu X, Li Z, Bao Z, Chen H, You Y, Kochanek PM, Yin H, Liu N, Kagan VE, Bayır H, Ji J, Cardiolipin-dependent Mitophagy guides outcome after traumatic brain injury, J. Neurosci 39 (2019) 1930–1943, 10.1523/JNEUROSCI.3415-17.2018. [PubMed: 30626699]

[11]. Simmons EC, Scholpa NE, Schnellmann RG, Mitochondrial biogenesis as a therapeutic target for traumatic and neurodegenerative CNS diseases, Exp. Neurol 329 (2020), 113309, 10.1016/j.expneurol.2020.113309. [PubMed: 32289315]

[12]. Gustafsson D, Klang A, Thams S, Rostami E, The role of BDNF in experimental and clinical traumatic brain injury, Int. J. Mol. Sci 22 (2021) 3582, 10.3390/ijms22073582. [PubMed: 33808272]

[13]. Nikoletopoulou V, Sidiropoulou K, Kallergi E, Dalezios Y, Tavernarakis N, Modulation of autophagy by BDNF underlies synaptic plasticity, Cell Metab. 26 (2017) 230–242.e5, 10.1016/j.cmet.2017.06.005. [PubMed: 28683289]

[14]. Krishna G, Agrawal R, Zhuang Y, Ying Z, Paydar A, Harris NG, Royes LFF, Gomez-Pinilla F, 7,8-Dihydroxyflavone facilitates the action exercise to restore plasticity and functionality: Implications for early brain trauma recovery, Biochimica et Biophysica Acta (BBA) - Molecular Basis of Disease. 1863 (2017) 1204–1213, 10.1016/j.bbadis.2017.03.007. [PubMed: 28315455]

[15]. Agrawal R, Tyagi E, Vergnes L, Reue K, Gomez-Pinilla F, Coupling energy homeostasis with a mechanism to support plasticity in brain trauma, Biochimica et Biophysica Acta (BBA) - Molecular Basis of Disease. 1842 (2014) 535–546, 10.1016/j.bbadis.2013.12.004. [PubMed: 24345766]

[16]. Zhou S-B, Xue M, Liu W, Chen Y-X, Chen Q-Y, Lu J-S, Wang J, Ye K, Li X-H, Zhuo M, Age-related attenuation of cortical synaptic tagging in the ACC is rescued by BDNF or a TrkB receptor agonist in both sex of mice, Mol Brain. 16 (2023) 4, 10.1186/s13041-022-00992-x. [PubMed: 36604761]

[17]. Walf AA, Frye CA, The use of the elevated plus maze as an assay of anxiety-related behavior in rodents, Nat. Protoc 2 (2007) 322–328, 10.1038/nprot.2007.44. [PubMed: 17406592]

[18]. Tucker LB, McCabe JT, Measuring anxiety-like behaviors in rodent models of traumatic brain injury, Front. Behav. Neurosci 15 (2021), 10.3389/fnbeh.2021.682935.

[19]. Thapak P, Khare P, Bishnoi M, Sharma SS, Neuroprotective effect of 2-Aminoethoxydiphenyl borate (2-APB) in amyloid β-induced memory dysfunction: a mechanistic study, Cell. Mol. Neurobiol 42 (2022) 1211–1223, 10.1007/s10571-020-01012-z. [PubMed: 33219878]

[20]. Acin-Perez R, Benador IY, Petcherski A, Veliova M, Benavides GA, Lagarrigue S, Caudal A, Vergnes L, Murphy AN, Karamanlidis G, Tian R, Reue K, Wanagat J, Sacks H, Amati F, Darley-Usmar VM, Liesa M, Divakaruni AS, Stiles L, Shirihai OS, A novel approach to measure mitochondrial respiration in frozen biological samples, EMBO J. 39 (2020), 10.15252/embj.2019104073.

[21]. Paydar A, Harris NG, The pericontused cortex can support function early after TBI but it remains functionally isolated from normal afferent input, Exp. Neurol 359 (2023), 114260, 10.1016/j.expneurol.2022.114260. [PubMed: 36404463]

[22]. Choe KY, Bethlehem RAI, Safrin M, Dong H, Salman E, Li Y, Grinevich V, Golshani P, DeNardo LA, Peñagarikano O, Harris NG, Geschwind DH, Oxytocin normalizes altered circuit connectivity for social rescue of the Cntnap2 knockout mouse, Neuron. 110 (2022) 795–808.e6, 10.1016/j.neuron.2021.11.031. [PubMed: 34932941]

[23]. Harris NG, Verley DR, Gutman BA, Thompson PM, Yeh HJ, Brown JA, Disconnection and hyper-connectivity underlie reorganization after TBI: a rodent functional connectomic analysis, Exp. Neurol 277 (2016) 124–138, 10.1016/j.expneurol.2015.12.020. [PubMed: 26730520]

[24]. Jenkinson M, Beckmann CF, Behrens TEJ, Woolrich MW, Smith SM, FSL. Neuroimage. 62 (2012) 782–790, 10.1016/j.neuroimage.2011.09.015. [PubMed: 21979382]

[25]. Smith SM, Jenkinson M, Woolrich MW, Beckmann CF, Behrens TEJ, Johansen-Berg H, Bannister PR, de Luca M, Drobnjak I, Flitney DE, Niazy RK, Saunders J, Vickers J, Zhang Y, de Stefano N, Brady JM, Matthews PM, Advances in functional and structural MR image analysis and implementation as FSL, Neuroimage. 23 (2004) S208–S219, 10.1016/j.neuroimage.2004.07.051. [PubMed: 15501092]

[26]. Woolrich MW, Jbabdi S, Patenaude B, Chappell M, Makni S, Behrens T, Beckmann C, Jenkinson M, Smith SM, Bayesian analysis of neuroimaging data in FSL, Neuroimage. 45 (2009) S173–S186, 10.1016/j.neuroimage.2008.10.055. [PubMed: 19059349]

[27]. Woolrich MW, Ripley BD, Brady M, Smith SM, Temporal autocorrelation in univariate linear modeling of FMRI data, Neuroimage. 14 (2001) 1370–1386, 10.1006/nimg.2001.0931. [PubMed: 11707093]

[28]. Woolrich MW, Behrens TEJ, Beckmann CF, Jenkinson M, Smith SM, Multilevel linear modelling for FMRI group analysis using Bayesian inference, Neuroimage. 21 (2004) 1732–1747, 10.1016/j.neuroimage.2003.12.023. [PubMed: 15050594]

[29]. Avants B, Tustison NJ, Song G, Advanced normalization tools: V1.0, Insight J. (2009), 10.54294/uvnhin.

[30]. Martin J-L, Finsterwald C, Cooperation between BDNF and glutamate in the regulation of synaptic transmission and neuronal development, Commun Integr Biol 4 (2011) 14–16, 10.4161/cib.13761. [PubMed: 21509169]

[31]. Choi SH, Li Y, Parada LF, Sisodia SS, Regulation of hippocampal progenitor cell survival, proliferation and dendritic development by BDNF, Mol. Neurodegener 4 (2009) 52, 10.1186/1750-1326-4-52. [PubMed: 20025751]

[32]. Lu B, Nagappan G, Lu Y, BDNF and Synaptic Plasticity, Cognitive Function, and Dysfunction, in: 2014: pp. 223–250. doi:10.1007/978-3-642-45106-5_9.

[33]. Agrawal R, Noble E, Tyagi E, Zhuang Y, Ying Z, Gomez-Pinilla F, Flavonoid derivative 7,8-DHF attenuates TBI pathology via TrkB activation, Biochimica et Biophysica Acta (BBA) - Molecular Basis of Disease. 1852 (2015) 862–872, 10.1016/j.bbadis.2015.01.018. [PubMed: 25661191]

[34]. Zhao S, Yu A, Wang X, Gao X, Chen J, Post-injury treatment of 7,8-Dihydroxyflavone promotes neurogenesis in the Hippocampus of the adult mouse, J. Neurotrauma 33 (2016) 2055–2064, 10.1089/neu.2015.4036. [PubMed: 26715291]

[35]. Wu C-H, Hung T-H, Chen C-C, Ke C-H, Lee C-Y, Wang P-Y, Chen S-F, Post-injury treatment with 7,8-Dihydroxyflavone, a TrkB receptor agonist, protects against experimental traumatic brain injury via PI3K/Akt signaling, PLoS One 9 (2014), e113397, 10.1371/journal.pone.0113397. [PubMed: 25415296]

[36]. Krishna G, Ying Z, Gomez-Pinilla F, Blueberry supplementation mitigates altered brain plasticity and behavior after traumatic brain injury in rats, Mol. Nutr. Food Res 63 (2019) 1801055, 10.1002/mnfr.201801055.

[37]. Martínez-Turrillas R, del Río J, Frechilla D, Sequential changes in BDNF mRNA expression and synaptic levels of AMPA receptor subunits in rat hippocampus after chronic antidepressant treatment, Neuropharmacology. 49 (2005) 1178–1188, 10.1016/j.neuropharm.2005.07.006. [PubMed: 16143352]

[38]. Isaac JTR, Ashby MC, McBain CJ, The role of the GluR2 subunit in AMPA receptor function and synaptic plasticity, Neuron. 54 (2007) 859–871, 10.1016/j.neuron.2007.06.001. [PubMed: 17582328]

[39]. Ehrlich I, Postsynaptic density 95 controls AMPA receptor incorporation during long-term potentiation and experience-driven synaptic plasticity, J. Neurosci 24 (2004) 916–927, 10.1523/JNEUROSCI.4733-03.2004. [PubMed: 14749436]

[40]. Jourdi H, Iwakura Y, Narisawa-Saito M, Ibaraki K, Xiong H, Watanabe M, Hayashi Y, Takei N, Nawa H, Brain-derived neurotrophic factor signal enhances and maintains the expression of AMPA receptor-associated PDZ proteins in developing cortical neurons, Dev. Biol 263 (2003) 216–230, 10.1016/j.ydbio.2003.07.008. [PubMed: 14597197]

[41]. Narisawa-Saito M, Iwakura Y, Kawamura M, Araki K, Kozaki S, Takei N, Nawa H, Brain-derived neurotrophic factor regulates surface expression of α-Amino-3-hydroxy-5-methyl-4-isoxazoleproprionic acid receptors by enhancing the N-Ethylmaleimide-sensitive factor/GluR2

interaction in developing neocortical neurons, J. Biol. Chem 277 (2002) 40901–40910, 10.1074/jbc.M202158200. [PubMed: 12130635]

[42]. Ansari MA, Roberts KN, Scheff SW, A time course of contusion-induced oxidative stress and synaptic proteins in cortex in a rat model of TBI, J. Neurotrauma 25 (2008) 513–526, 10.1089/neu.2007.0451. [PubMed: 18533843]

[43]. Kida S, A functional role for CREB as a positive regulator of memory formation and LTP, Exp Neurobiol. 21 (2012) 136–140, 10.5607/en.2012.21.4.136. [PubMed: 23319873]

[44]. Tao X, Finkbeiner S, Arnold DB, Shaywitz AJ, Greenberg ME, Ca2+ influx regulates BDNF transcription by a CREB family transcription factor-dependent mechanism, Neuron. 20 (1998) 709–726, 10.1016/S0896-6273(00)81010-7. [PubMed: 9581763]

[45]. Ahmed S, Kwatra M, Gawali B, Panda SR, Naidu VGM, Potential role of TrkB agonist in neuronal survival by promoting CREB/BDNF and PI3K/Akt signaling in vitro and in vivo model of 3-nitropropionic acid (3-NP)-induced neuronal death, Apoptosis. 26 (2021) 52–70, 10.1007/s10495-020-01645-x. [PubMed: 33226552]

[46]. Ohira K, Hayashi M, A new aspect of the TrkB signaling pathway in neural plasticity, Curr. Neuropharmacol 7 (2009) 276–285, 10.2174/157015909790031210. [PubMed: 20514207]

[47]. Panja D, Bramham CR, BDNF mechanisms in late LTP formation: a synthesis and breakdown, Neuropharmacology. 76 (2014) 664–676, 10.1016/j.neuropharm.2013.06.024. [PubMed: 23831365]

[48]. Yoshii A, Constantine-Paton M, Postsynaptic BDNF-TrkB signaling in synapse maturation, plasticity, and disease, Dev Neurobiol. (2010), 10.1002/dneu.20765. NA–NA.

[49]. Teng HK, ProBDNF induces neuronal apoptosis via activation of a receptor complex of p75NTR and Sortilin, J. Neurosci 25 (2005) 5455–5463, 10.1523/JNEUROSCI.5123-04.2005. [PubMed: 15930396]

[50]. Ahmed S, Kwatra M, Gawali B, Panda SR, Naidu VGM, Potential role of TrkB agonist in neuronal survival by promoting CREB/BDNF and PI3K/Akt signaling in vitro and in vivo model of 3-nitropropionic acid (3-NP)-induced neuronal death, Apoptosis. 26 (2021) 52–70, 10.1007/s10495-020-01645-x. [PubMed: 33226552]

[51]. Woo NH, Teng HK, Siao C-J, Chiaruttini C, Pang PT, Milner TA, Hempstead BL, Lu B, Activation of p75NTR by proBDNF facilitates hippocampal long-term depression, Nat. Neurosci 8 (2005) 1069–1077, 10.1038/nn1510. [PubMed: 16025106]

[52]. Thomas AX, Cruz Del Angel Y, Gonzalez MI, Carrel AJ, Carlsen J, Lam PM, Hempstead BL, J. Russek Shelley, Brooks-Kayal AR, Rapid increases in proBDNF after pilocarpine-induced status epilepticus in mice are associated with reduced proBDNF cleavage machinery, ENeuro. 3 (2016), 10.1523/ENEURO.0020-15.2016. ENEURO.0020–15.2016.

[53]. Pang PT, Teng HK, Zaitsev E, Woo NT, Sakata K, Zhen S, Teng KK, Yung W-H, Hempstead BL, Lu B, Cleavage of proBDNF by tPA/plasmin is essential for long-term hippocampal plasticity, Science 306 (2004) (1979) 487–491, 10.1126/science.1100135. [PubMed: 15486301]

[54]. Xia Y, Pu H, Leak RK, Shi Y, Mu H, Hu X, Lu Z, Foley LM, Hitchens TK, Dixon CE, Bennett MVL, Chen J, Tissue plasminogen activator promotes white matter integrity and functional recovery in a murine model of traumatic brain injury, Proc. Natl. Acad. Sci 115 (2018), 10.1073/pnas.1810693115.

[55]. Ding Q, Ying Z, Gomez-Pinilla F, Exercise influences hippocampal plasticity by modulating brain-derived neurotrophic factor processing, Neuroscience. 192 (2011) 773–780, 10.1016/j.neuroscience.2011.06.032. [PubMed: 21756980]

[56]. Podyma B, Parekh K, Güler AD, Deppmann CD, Metabolic homeostasis via BDNF and its receptors, Trends in Endocrinology & Metabolism. 32 (2021) 488–499, 10.1016/j.tem.2021.04.005. [PubMed: 33958275]

[57]. Gilmer LK, Roberts KN, Joy K, Sullivan PG, Scheff SW, Early mitochondrial dysfunction after cortical contusion injury, J. Neurotrauma 26 (2009) 1271–1280, 10.1089/neu.2008.0857. [PubMed: 19637966]

[58]. Li X, Wang H, Gao Y, Li L, Tang C, Wen G, Yang Y, Zhuang Z, Zhou M, Mao L, Fan Y, Quercetin induces mitochondrial biogenesis in experimental traumatic brain injury via the PGC-1α signaling pathway, Am. J. Transl. Res 8 (2016) 3558–3566. [PubMed: 27648146]

[59]. Markham A, Cameron I, Franklin P, Spedding M, BDNF increases rat brain mitochondrial respiratory coupling at complex I, but not complex II, Eur. J. Neurosci 20 (2004) 1189–1196, 10.1111/j.1460-9568.2004.03578.x. [PubMed: 15341590]

[60]. Jin H, Zhu Y, Li Y, Ding X, Ma W, Han X, Wang B, BDNF-mediated mitophagy alleviates high-glucose-induced brain microvascular endothelial cell injury, Apoptosis. 24 (2019) 511–528, 10.1007/s10495-019-01535-x. [PubMed: 30877409]

[61]. Rai SN, Singh C, Singh A, Singh MP, Singh BK, Mitochondrial dysfunction: a potential therapeutic target to treat Alzheimer's disease, Mol. Neurobiol 57 (2020) 3075–3088, 10.1007/s12035-020-01945-y. [PubMed: 32462551]

[62]. Zuo L, Dai C, Yi L, Dong Z, 7,8-Dihydroxyflavone ameliorates motor deficits via regulating autophagy in MPTP-induced mouse model of Parkinson's disease, Cell Death Discov. 7 (2021) 254, 10.1038/s41420-021-00643-5. [PubMed: 34545064]

[63]. Xu Z, Lv X-A, Dai Q, Lu M, Jin Z, Exogenous BDNF increases mitochondrial pCREB and alleviates neuronal metabolic defects following mechanical injury in a MPTP-dependent way, Mol. Neurobiol 55 (2018) 3499–3512, 10.1007/s12035-017-0576-5. [PubMed: 28508150]

[64]. Li J, Lai M, Zhang X, Li Z, Yang D, Zhao M, Wang D, Sun Z, Ehsan S, Li W, Gao H, Zhao D, Yang L, PINK1-parkin-mediated neuronal mitophagy deficiency in prion disease, Cell Death Dis. 13 (2022) 162, 10.1038/s41419-022-04613-2. [PubMed: 35184140]

[65]. Quinn PMJ, Moreira PI, Ambrosio AF, Alves CH, PINK1/PARKIN signalling in neurodegeneration and neuroinflammation, Acta Neuropathol Commun. 8 (2020) 189, 10.1186/s40478-020-01062-w. [PubMed: 33168089]

[66]. Tanida I, Ueno T, Kominami E, LC3 and Autophagy, 2008, pp. 77–88, 10.1007/978-1-59745-157-4_4.

[67]. Jin SM, Youle RJ, PINK1- and Parkin-mediated mitophagy at a glance, J. Cell Sci 125 (2012) 795–799, 10.1242/jcs.093849. [PubMed: 22448035]

[68]. Lee Y, Lee H-Y, Hanna RA, Gustafsson ÅB, Mitochondrial autophagy by Bnip3 involves Drp1-mediated mitochondrial fission and recruitment of Parkin in cardiac myocytes, American Journal of Physiology-Heart and Circulatory Physiology. 301 (2011) H1924–H1931, 10.1152/ajpheart.00368.2011. [PubMed: 21890690]

[69]. Shi R-Y, Zhu S-H, Li V, Gibson SB, Xu X-S, Kong J-M, BNIP3 interacting with LC3 triggers excessive Mitophagy in delayed neuronal death in stroke, CNS Neurosci Ther. 20 (2014) 1045–1055, 10.1111/cns.12325. [PubMed: 25230377]

[70]. Dibble CC, Cantley LC, Regulation of mTORC1 by PI3K signaling, Trends Cell Biol. 25 (2015) 545–555, 10.1016/j.tcb.2015.06.002. [PubMed: 26159692]

[71]. Bartolome A, García-Aguilar A, Asahara S-I, Kido Y, Guillen C, Pajvani UB, Benito M, MTORC1 regulates both general autophagy and Mitophagy induction after oxidative phosphorylation uncoupling, Mol. Cell. Biol 37 (2017), 10.1128/MCB.00441-17.

[72]. Lipton PA, Eichenbaum H, Complementary roles of Hippocampus and medial entorhinal cortex in episodic memory, Neural Plast. 2008 (2008) 1–8, 10.1155/2008/258467.

[73]. Strauch C, Manahan-Vaughan D, Orchestration of hippocampal information encoding by the piriform cortex, Cereb. Cortex 30 (2020) 135–147, 10.1093/cercor/bhz077. [PubMed: 31220213]

[74]. Toi PT, Jang HJ, Min K, Kim S-P, Lee S-K, Lee J, Kwag J, Park J-Y, In vivo direct imaging of neuronal activity at high temporospatial resolution, Science 378 (2022) (1979) 160–168, 10.1126/science.abh4340. [PubMed: 36227975]

[75]. Jung WB, Jiang H, Lee S, Kim S-G, Dissection of brain-wide resting-state and functional somatosensory circuits by fMRI with optogenetic silencing, Proc. Natl. Acad. Sci 119 (2022), 10.1073/pnas.2113313119.

[76]. Wu R, Yang P-F, Chen LM, Correlated disruption of resting-state fMRI, LFP, and spike connectivity between area 3b and S2 following spinal cord injury in monkeys, J. Neurosci 37 (2017) 11192–11203, 10.1523/JNEUROSCI.2318-17.2017. [PubMed: 29038239]

[77]. Valenti D, Stagni F, Emili M, Guidi S, Bartesaghi R, Vacca RA, Impaired brain mitochondrial bioenergetics in the Ts65Dn mouse model of down syndrome is restored by neonatal treatment with the polyphenol 7,8-Dihydroxyflavone, Antioxidants. 11 (2021) 62, 10.3390/antiox11010062. [PubMed: 35052567]

[78]. Li T, Li X, Huang X, Yu H, Li S, Zhang Z, Xie Y, Song X, Liu J, Yang X, Liu G, Mitochondriomics reveals the underlying neuroprotective mechanism of TrkB receptor agonist R13 in the 5×FAD mice, Neuropharmacology. 204 (2022), 108899, 10.1016/j.neuropharm.2021.108899. [PubMed: 34838815]

[79]. Tabrizi P, Wang L, Seeds N, McComb JG, Yamada S, Griffin JH, Carmeliet P, Weiss MH, Zlokovic BV, Tissue plasminogen activator (tPA) deficiency exacerbates cerebrovascular fibrin deposition and brain injury in a murine stroke model, Arterioscler Thromb Vasc Biol. 19 (1999) 2801–2806. doi:10.1161/01.ATV.19.11.2801. [PubMed: 10559029]

[80]. Kallakuri S, Bandaru S, Zakaria N, Shen Y, Kou Z, Zhang L, Haacke EM, Cavanaugh JM, Traumatic brain injury by a closed head injury device induces cerebral blood flow changes and microhemorrhages, J Clin Imaging Sci. 5 (2015) 52, 10.4103/2156-7514.166354. [PubMed: 26605126]

[81]. Hillman EMC, Coupling mechanism and significance of the BOLD signal: a status report, Annu. Rev. Neurosci 37 (2014) 161–181, 10.1146/annurev-neuro-071013-014111. [PubMed: 25032494]

[82]. Gravanis I, Tsirka SE, Tissue-type plasminogen activator as a therapeutic target in stroke, Expert Opin. Ther. Targets 12 (2008) 159–170, 10.1517/14728222.12.2.159. [PubMed: 18208365]

[83]. Englund EK, Langham MC, Quantitative and dynamic MRI measures of peripheral vascular function, Front. Physiol 11 (2020), 10.3389/fphys.2020.00120.

[84]. Li X, Chen C, Zhan X, Li B, Zhang Z, Li S, Xie Y, Song X, Shen Y, Liu J, Liu P, Liu G-P, Yang X, R13 preserves motor performance in SOD1 ^{G93A} mice by improving mitochondrial function, Theranostics. 11 (2021) 7294–7307, 10.7150/thno.56070. [PubMed: 34158851]

[85]. A controlled trial of recombinant methionyl human BDNF in ALS, Neurology. 52 (1999) 1427–1433, 10.1212/WNL.52.7.1427. [PubMed: 10227630]

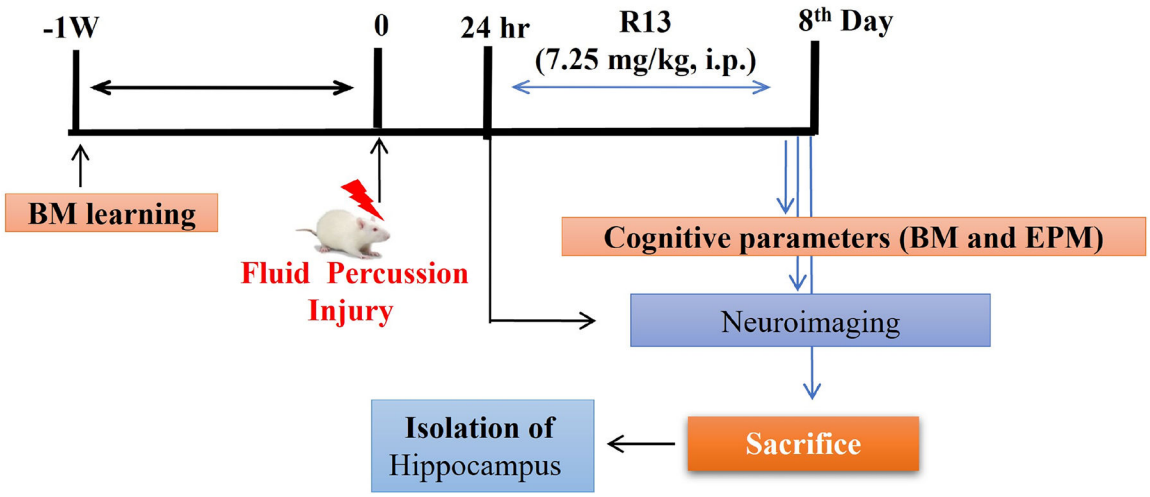

Fig. 1.

Schematic representation of the experimental design. All animals received a learning trial (two trial per day) for consecutive 5 days after that FPI and sham surgery was performed. After 24 h of post-TBI all animals went for MRI imaging and after imaging R13 (7.25 mg/kg, i.p.) was administered for 7 days daily. On the 6th and 7th day post-TBI, the Barnes maze and elevated plus maze were performed respectively after that MRI imaging was performed. Following the next day, animals were harvested, and the hippocampus was isolated for further expression study.

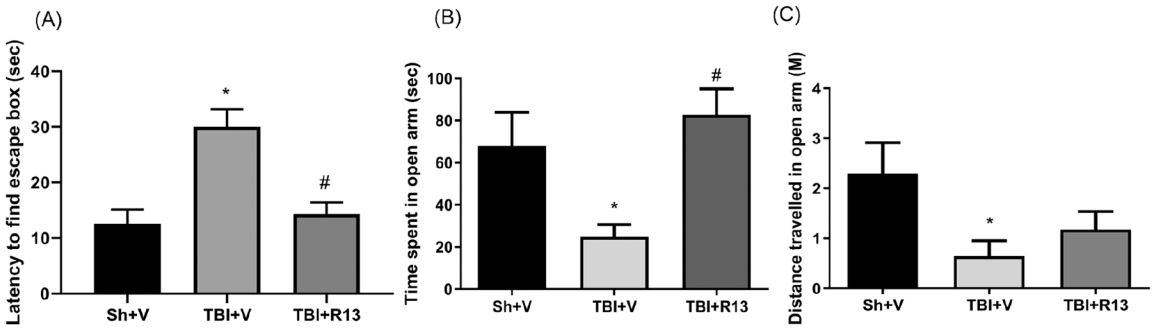

Fig. 2.

Effects of R13 on spatial learning and anxiety-like behavior assessment (A) Escape latency to find an escape box in the BM test (B) Time spent in open arm in EPM (C) Distance travelled in the open arm during EPM test. Values are expressed as mean ± SEM, $n = 5–7$. Statistical significance was analyzed by one-way ANOVA followed by a post hoc Dunn's test. *P 0.05 vs sham-operated animals, #P 0.01 vs FPI-operated animals.

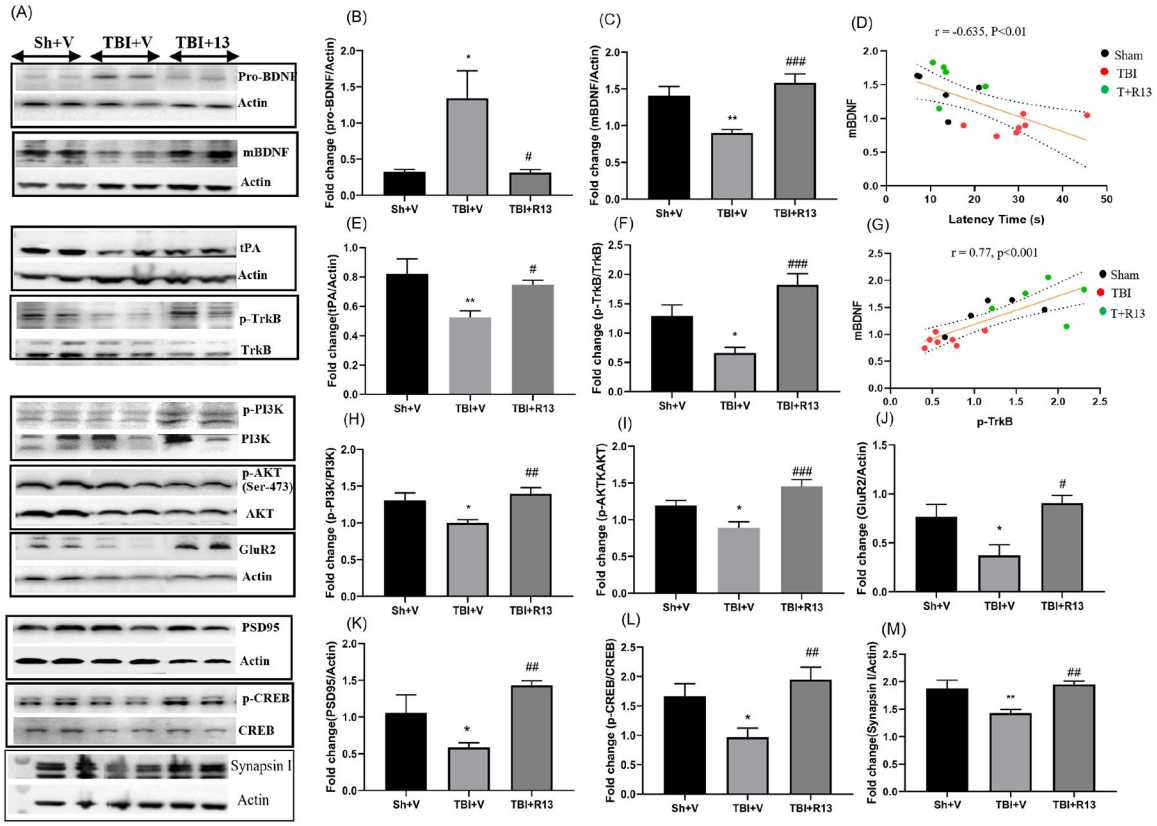

Fig. 3.

Effects of R13 on BDNF/TrkB signaling post-TBI in the hippocampus. (A) Representation of immunoblots (B) Protein level of pro-BDNF (C) Protein level of mBDNF (D) Correlation between mBDNF and BM latency (E) Protein level of tPA (F) Protein level of p-TrkB (G) Correlation between mBDNF and p-TrkB (H) Protein level of p-PI3K (I) Protein level of p-Akt (L) Protein level of GluR2 (K) Protein level of PSD-95 (L) Protein level of p-CREB (M) Protein level of synapsin I in the hippocampus. Values are expressed as mean ± SEM, n = 5–7. Statistical significance was analyzed by one-way ANOVA followed by a post hoc Tukey's test. **P 0.01, *P 0.05 vs sham-operated animals, #P 0.01, ##P 0.01, ###*P* 0.001 vs FPI-operated animals.

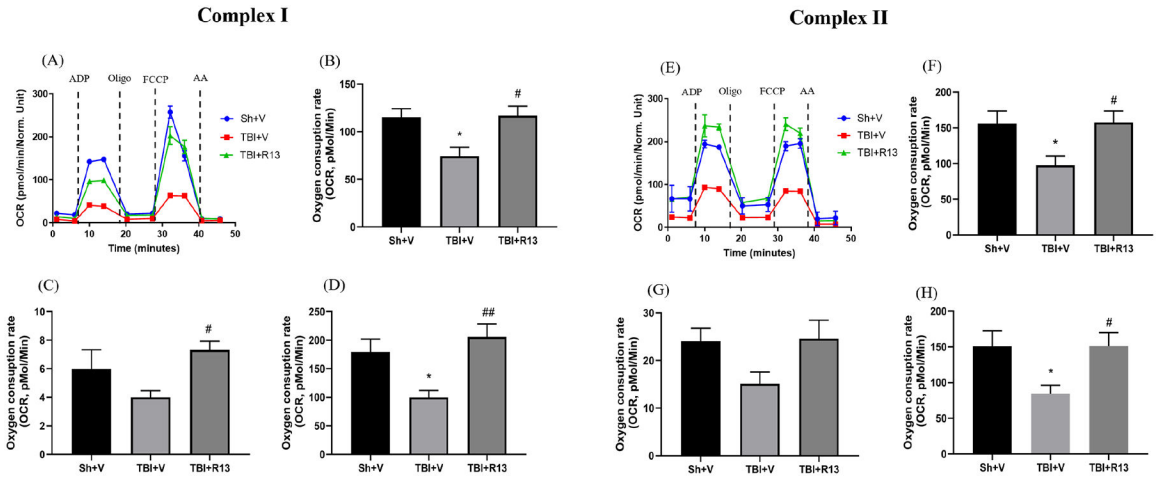

Fig. 4.

Effects of R13 on mitochondrial homeostasis and mitophagy signaling post-TBI. (A) Representation of immunoblots (B) Protein level of PGC-1α (C) Protein level of SOD (D) Correlation between PGC-1α and BM latency (E) Protein level of TOM20 (F) Protein level of PINK1 (G) Protein level of parkin (H) Protein level of MAP-LC3β (I) Protein level of BNIP3 in the hippocampus (J) Correlation between BNIP3 and BM latency (K) Correlation between mBDNF and BNIP3 (L) Correlation between BNIP3 and SOD. Values are expressed as mean ± SEM, n = 5–7. Statistical significance was analyzed by one-way ANOVA followed by a post hoc Tukey's test. *P 0.05, ***P 0.001vs sham-operated animals, #P 0.05, ##P 0.001, ###P 0.001 vs FPI-operated animals.

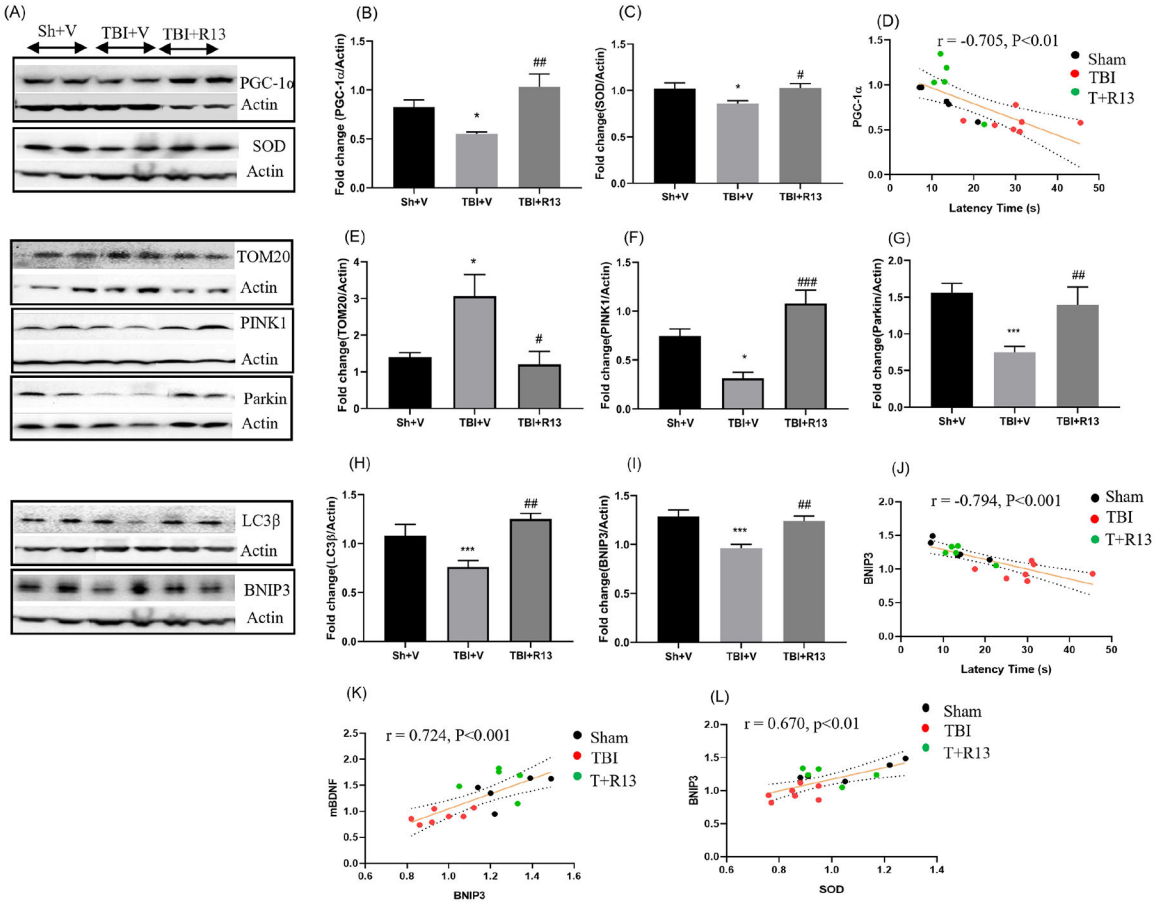

Fig. 5.

R13 treatment results in increased brain connectivity based on left hippocampal seed analysis of resting state MRI. (A-C) Group comparisons of mean increase in connectivity over time, heat map shows z-value of group comparison of left hippocampal seed connectivity increase of time. (A) Increase connectivity from seed in FPI vehicle compared to sham. (B) Increased connectivity with R13 compared to sham. (C) Increased connectivity with R13 intervention compared to vehicle. (D) Summary of increased connectivity following 1 week of R13 treatment post-injury when compared to shams. Analysis is exploratory based on uncorrected statistics with a minimum z of 1.7 (p 0.05). Ac-nucleus accumbens, Ai-agranular insular cortex, Bs-Brain stem, Hy-hypothalamus, Hp-Hippocampus, Mb-rest of the midbrain, Me-medial entorhinal cortex, Pi- Piriform cortex, Pr-Prelimbic, Rs-retrospienial Cortex, S1-primary somatosensory cortex, Sa-Striatum, Th-thalamus.

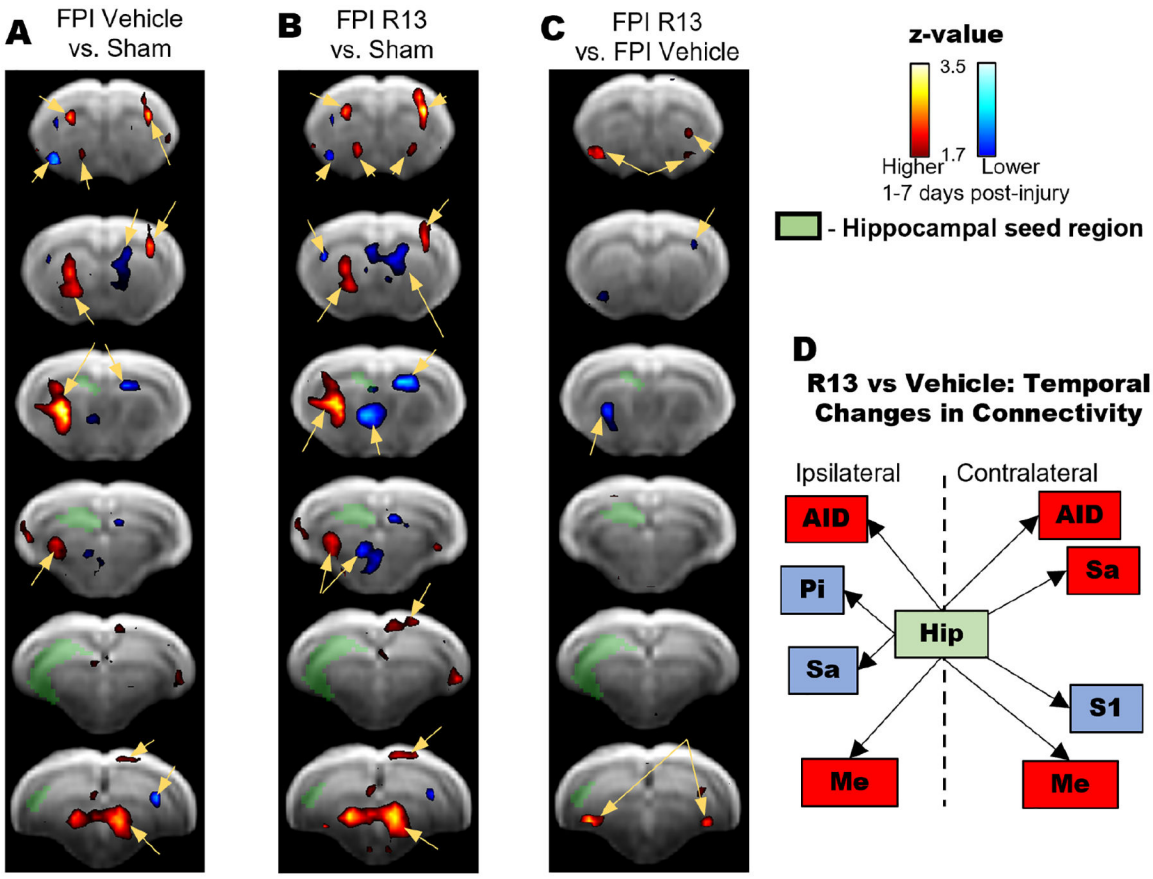

Fig. 6.

R13 treatment results in increased brain connectivity based on left hippocampal seed analysis of resting state MRI. (A-C) Group comparisons of mean changes in connectivity over time, heat map shows z-value of group comparison of left hippocampal seed connectivity increase of time. (A, B) Red heatmap indicates a greater increase over time for FPI compared to shams. Blue heatmap indicates a lower change over time for FPI compared to shams, (C) Red heatmap indicates a greater increase in connectivity overtime for FPI-R13 compared to FPI-vehicle. Blue heatmap indicates a lower change over time for FPI-R13 compared to FPI-vehicle. (D) Summary of temporal changes in connectivity in regions functionally connected to the hippocampus following 1 week of R13 treatment compared to vehicle (red and blue indicate higher and lower changes over time respectively, compared to vehicle). This analysis is exploratory and it is based on uncorrected statistics with a minimum z of 1.7 (p 0.05). Key: Ac-nucleus accumbens, AID- Agranular insular cortex, Di- dysgranular insular cortex, Hp-Hippocampus, M1-primary motor cortex, Mb-rest of the midbrain, Me-medial entorhinal cortex, Pi- Piriform cortex, Rs-retrosplenial Cortex, S1-primary somatosensory cortex, Sa-Striatum, Th-thalamus.

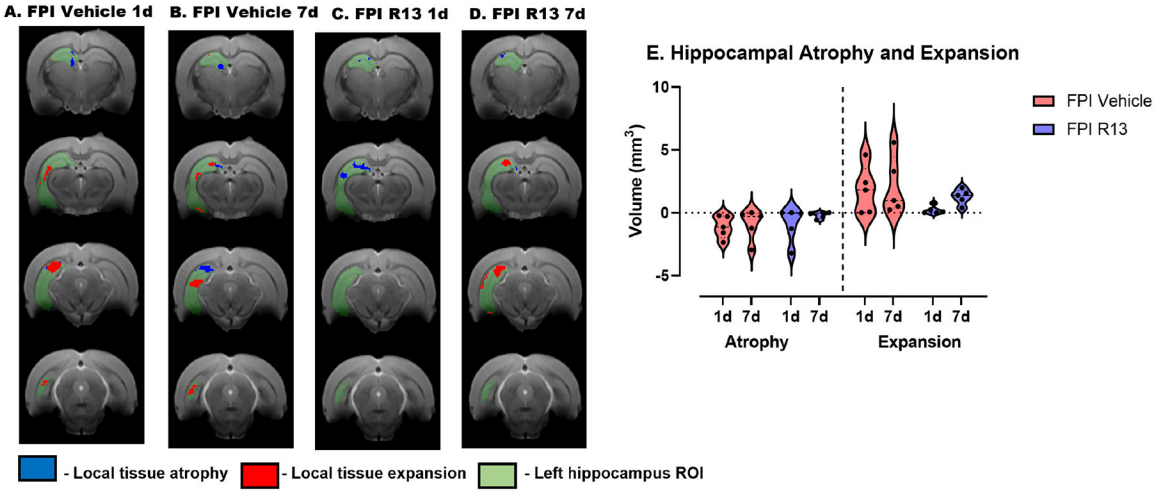

Fig. 7.

R13 treatment trended toward lower hippocampal atrophy. (A-D) Area in the left hippocampus where at least one animal had significant atrophy or expansion when compared to sham animals. (E) Volume of significant atrophy or expansion when compared to sham animals. Volumes are based on voxel-wise z score maps created by comparing to sham animals and applying a threshold of $z \geq 2.33$. No significant group effect is observed but R13 treatment tends to reduce the variance in the amount of significant atrophy after 1 week of treatment.

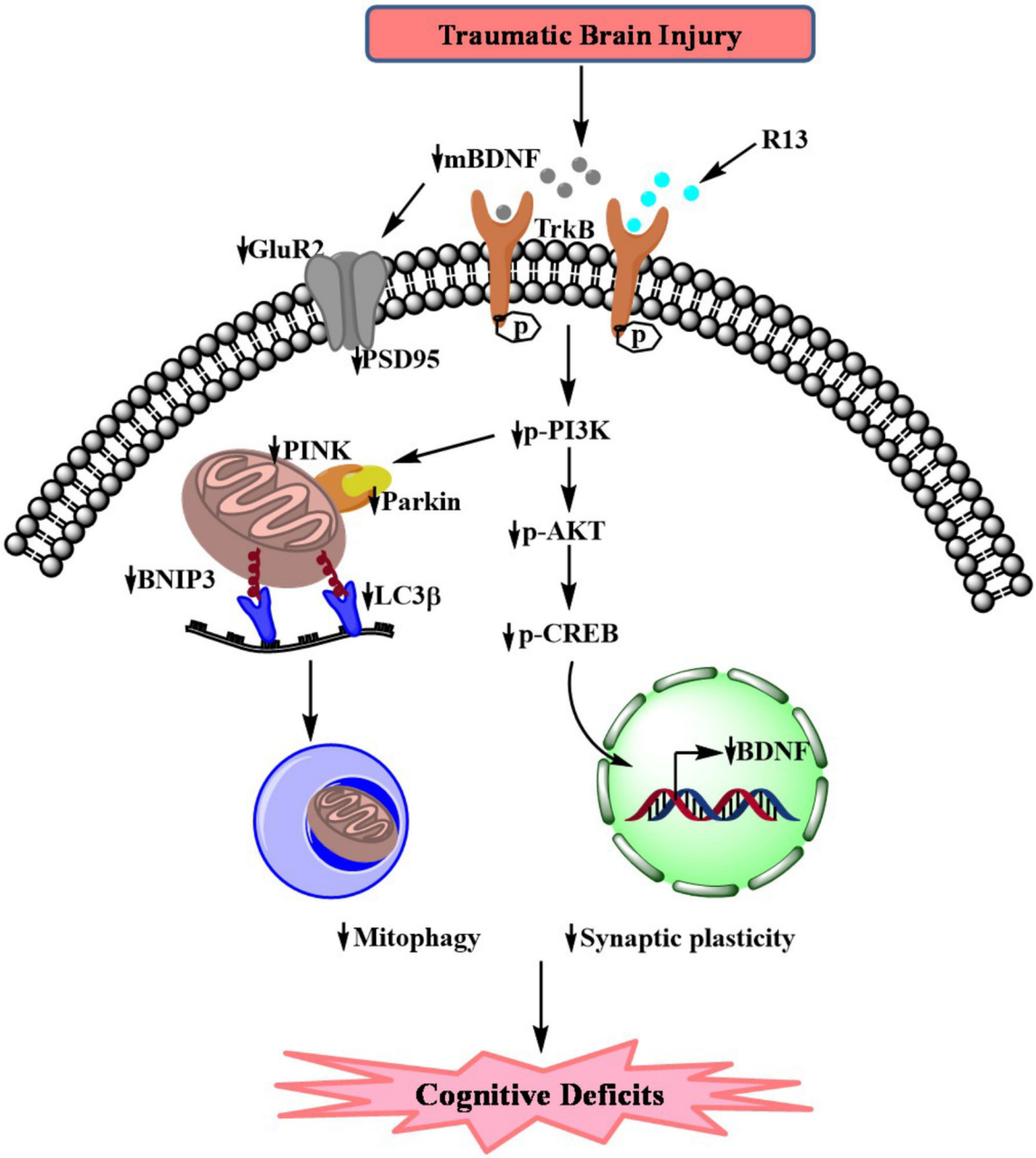

Fig. 8.

Postulated role of R13 on TBI pathology. A schematic representation shows that TBI state reduces mBDNF and TrkB signaling axis. TBI also affects mitochondrial function by reducing mitophagy in the hippocampus. R13, as BDNF mimetic enhances phosphorylation of TrkB receptor and downstream signaling (PI3K/Akt), and the phosphorylation of p-CREB. In addition, R13 intervention increased expression of synaptic proteins like PSD-95 and GluR2. R13 also restores mitochondrial mitophagy by enhancing the protein levels of PINK1, Parkin, BNIP3, and LC3β. Overall, R13 treatment appears to restore cognitive

function after TBI by acting on the TrkB/PI3K axis and enhancing mitochondrial dynamics in the brain.